



6

Normative Measurements of Head and Neck Lymph Nodes on Imaging

Grayson W. Hooper and
Daniel Thomas Ginat

6.1 Imaging Modalities

6.1.1 Computed Tomography (CT)

- CT soft tissue images with 1–3 mm section thickness can be used to accurately determine the location, size, and gross morphology of head and neck lymph nodes.
- Normal lymph nodes have attenuation similar to that of muscle.
- Intravenous contrast administration can help with characterization of lymph node consistency, such as the presence of necrosis.

G. W. Hooper
Department of Radiology, Fort Belvoir Community Hospital,
Fort Belvoir, VA, USA

D. T. Ginat (✉)
Department of Radiology, Section of Neuroradiology, University of
Chicago, Chicago, IL, USA
e-mail: dtg1@uchicago.edu

6.1.2 Magnetic Resonance Imaging (MRI)

- Normal lymph nodes display homogeneous T1 and T2 signal and enhancement.
- The optimal contrast between abnormal lymph nodes and muscle is achieved using a long repetition time (TR) and a long echo time (TE), although greater signal-to-noise ratio in MRI is achieved using a long TR and a short TE.
- Diffusion-weighted imaging (DWI) can be helpful in detecting subcentimeter metastatic lymph nodes in the setting of head and neck cancer, in which metastatic cervical lymph nodes generally have lower diffusivity as compared with benign lymph nodes.
- MRI contrast resolution is superior to that of CT and therefore is more sensitive for the detection of extracapsular spread than CT, as well as for discerning retropharyngeal lymph nodes, but MRI is generally not as reliable as CT for delineating lower neck lymph nodes due to the frequent presence of artifacts.

6.1.3 Ultrasound

- Ultrasound is used adjunctively in the evaluation of head and neck neoplasms and nodal metastasis.
- Ultrasound has the advantage of dynamic real time soft tissue evaluation, which can show detailed lymph node characteristics.
- Ultrasound has been shown to have both higher sensitivity and specificity for nodal metastasis when compared to CT.
- Ultrasound is limited in evaluating the deep lymph nodes of the neck. It is also user dependent, which contributes to imaging variability.

- The addition of ultrasound to CT can spare patients secondary surgery after sentinel node biopsy.

6.1.4 ¹⁸Fluoro-2-Deoxy-D-Glucose Positron Emission Tomography (¹⁸FDG-PET)

- ¹⁸FDG-PET provides an assessment of soft tissue metabolism through standardized uptake values (SUV) and has a higher sensitivity and specificity than CT for the detection of lymph node metastases in patients with head and neck cancer, but is routinely combined with CT or MRI for greater anatomic delineation.
- A lymph node SUV_{max}/liver SUV_{max} ratio ≥ 0.90 can be used as a threshold for detecting cervical metastatic nodes with an accuracy of 90%.
- ¹⁸FDG-PET can reliably detect metastatic neck lymph nodes that measure ≥ 10 mm, but intranodal tumor or metastatic lymph nodes smaller than 5 mm are generally not detectable.
- Regardless of size, certain cancers tend not to be FDG avid, such as adenoid cystic carcinomas.

6.2 RECIST Criteria

The response evaluation criteria in solid tumors (RECIST) was created in 2000 and updated in 2009 as a means of objectively measuring solid tumor response to therapy. Updated guidelines (RECIST 1.1) measure the longest dimension of the target lesion and the shortest dimension of lymph nodes in the axial plane with a minimum threshold of 15 mm. This measurement strategy also pertains to the most recent iRECIST guidelines for immunotherapy response. The short axis is determined by first identifying the long axis or the longest diameter of a lymph node and then measuring

Lymph Node Measurement Approach

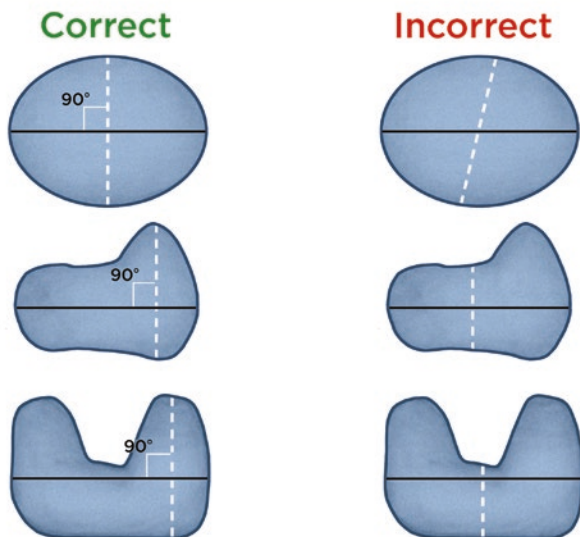


Fig. 6.1 Illustration depicting correct and incorrect approaches for measuring lymph nodes

the widest perpendicular diameter (Fig. 6.1). Similarly, if abnormal lymph nodes have coalesced such that they are no longer separable, the vector of the longest diameter of the overall lesion should be used to determine the perpendicular vector for the maximal short-axis diameter of the coalesced lesion (Fig. 6.2). Coalescent lymphadenopathy is an independent risk factor for poor prognosis in the setting of oropharyngeal squamous cell carcinoma.

6.3 Lymph Node Stations

6.3.1 Cervical Lymph Nodes

The cervical lymph node levels are delineated by recognizable anatomic landmarks, as illustrated in Fig. 6.3.

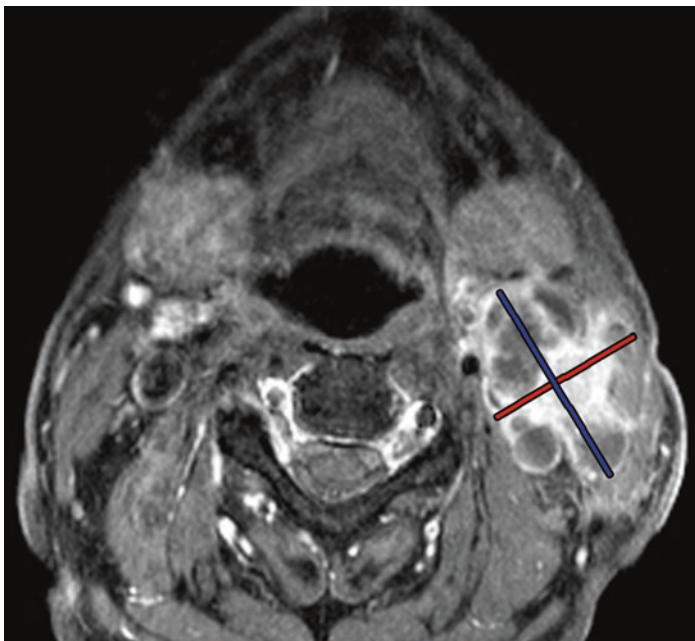


Fig. 6.2 Axial post-contrast T1-weighted magnetic resonance imaging (MRI) image shows a conglomerate of necrotic left cervical lymph node metastases with long axis (blue line) and short axis (red line) dimensions

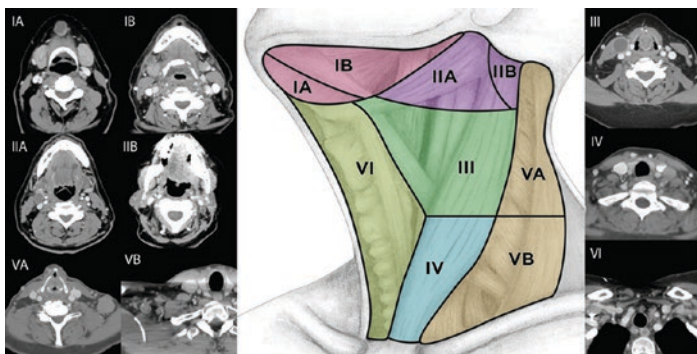


Fig. 6.3 Diagram of the cervical lymph node levels

If the short axis exceeds 11 mm in the jugulodigastric region and 10 mm in all other lateral compartment cervical nodes, and 8 mm for central compartment lymph nodes, metastasis is probably present in adults. The normal maximum long-axis size of jugulodigastric nodes in cancer patients is 15 mm. However, level 2 lymph nodes can normally measure up to 15 mm or more in children (Fig. 6.4). In addition, a ratio between the long- and short-axis diameters of less than 1.5, or a rounded lymph node, is suggestive of metastatic disease. Nevertheless, there is an error rate of 10–20% based on size criteria alone. Ultimately, there is a tradeoff between sensitivity and specificity for size thresholds. Indeed, up to 50% of lymph nodes measuring less than 5 mm har-



Fig. 6.4 Normal cervical lymph nodes in a child. Axial T2-weighted magnetic resonance imaging (MRI) shows plump cervical lymph nodes bilaterally along with tonsillar tissues in a 3-year-old infant without lymph node disease



Fig. 6.5 Reactive lymph node. Axial computed tomography (CT) image shows an enlarged right level 2 lymph node associated with right mandibular odontogenic infection

bor micrometastases that are occult on imaging. Alternatively, lymph node enlargement can result from benign inflammatory or reactive processes (Fig. 6.5).

Other features to consider besides size on imaging include the presence of cystic or necrotic components and effacement of the fatty hilum (Fig. 6.6). ^{18}F FDG-PET can sometimes be helpful in detecting hypermetabolic metastatic lymphadenopathy that is smaller than size criteria. The presence of calcifications can also be a sign of metastatic disease, particularly in the setting of thyroid cancer (Fig. 6.7). Extracapsular spread is another feature of

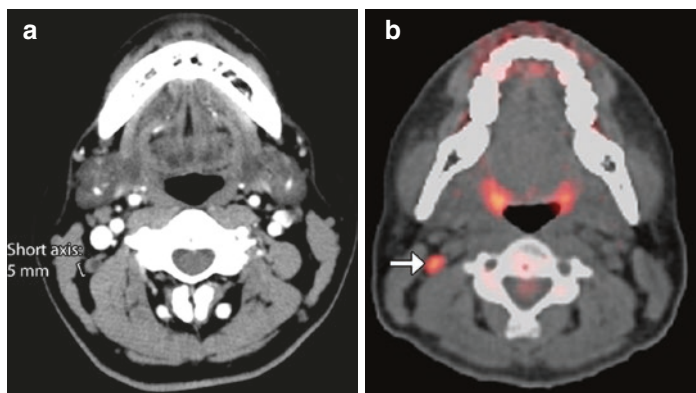


Fig. 6.6 Necrotic lymph node. Axial computed tomography (CT) image (a) shows a small right level 2B lymph node with a hypoattenuating area in a patient with nasopharyngeal carcinoma, which proved to be metastatic disease. The corresponding ^{18}F FDG-PET/CT image (b) shows the small lymph node is hypermetabolic (arrow)

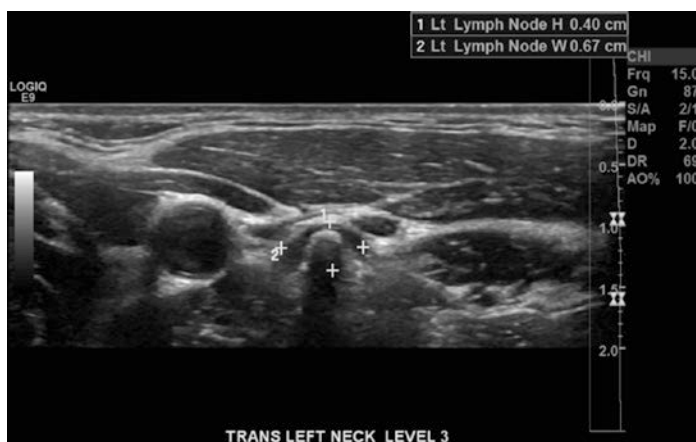


Fig. 6.7 Lymph node with calcification from metastatic thyroid cancer. Gray-scale ultrasound image shows the calcification with shadowing within a small level 3 lymph node

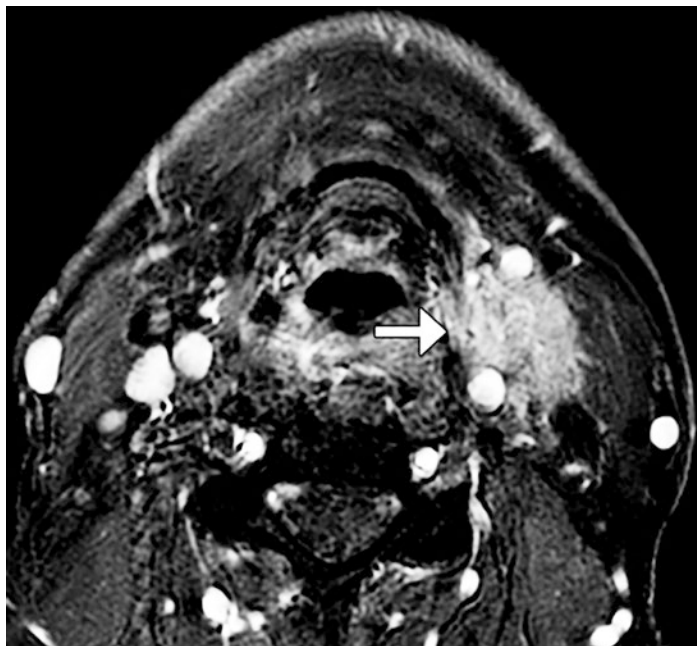


Fig. 6.8 Extracapsular spread. Axial post-contrast T1-weighted magnetic resonance imaging (MRI) shows a left cervical lymph node with infiltrative margins (arrow)

malignant lymphadenopathy that portends a relatively poor prognosis and is characterized by the presence of irregular margins and loss of adjacent fat planes, which is best delineated via MRI (Fig. 6.8). Furthermore, it is important to consider the presence of nodal grouping, which refers to three or more contiguous and confluent lymph nodes, each of which has a maximal diameter of 6–15 mm (Fig. 6.9). Such a grouping in the drainage chain of the tumor is suggestive of metastatic disease.

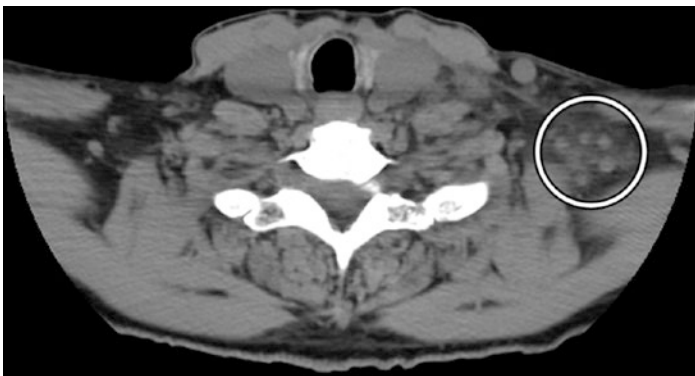


Fig. 6.9 Nodal grouping. Axial computed tomography (CT) image shows a cluster of left supraclavicular subcentimeter lymph nodes, which proved to be metastatic disease

Level I: Submental and Submandibular

- This nodal level is bounded by the mylohyoid muscle superiorly and the inferior margin of the hyoid inferiorly. It is further subdivided into sections “A” and “B” with level IA described as submental, between the anterior bellies of the digastric musculature. Level IB or submandibular lymph nodes are found posterolateral to the digastric muscles and anterior to the submandibular glands.
- The submental lymph nodes receive lymphatic drainage from:
 - Central inferior lip
 - Apex of the tongue
 - Floor of the mouth
- The submandibular lymph nodes receive lymphatic drainage from:
 - Facial lymph nodes
 - Cheeks
 - Lateral aspects of the nose
 - Oral cavity
 - Submental nodes
- Submandibular lymph nodes can assume a more rounded configuration ($S/L > 0.5$), which is different from the oval shape expected in other nodal stations (3).

Level II: Anterior Cervical/Upper Jugular

- This station is bounded superiorly by the base of the skull and inferiorly by the hyoid bone. It is bounded posteriorly by the posterior margin of the sternocleidomastoid and anteriorly by the posterior margin of the submandibular glands. Level II lymph nodes can be further subdivided into IIA and IIB. Level IIA lymph nodes are located posterior or otherwise tangent to the internal jugular vein. Level IIB lymph nodes are located posterior to the internal jugular vein and are separated from it by a fat plane.
- Level II lymph nodes receive lymphatic drainage from:
 - Oropharynx
 - Posterior aspect of the mouth
 - Parotid glands

Level III: Middle Jugular

- These lymph nodes are bounded superiorly by the inferior margin of the hyoid and inferiorly by the superior margin of the cricoid cartilage. The posterior boundary is posterior margin of the sternocleidomastoid muscle.
- The lymph nodes of this station receive lymphatic drainage from:
 - Larynx
 - Hypopharynx

Level IV: Inferior Jugular

- The inferior jugular lymph nodes are demarcated superiorly by the inferior margin of the cricoid cartilage and inferiorly by the superior surface of the clavicle. They are bounded anteriorly by the internal or common carotid artery, which separates level IV from level VI lymph nodes.
- Level IV lymph nodes receive lymphatic drainage from:
 - Subglottic soft tissues
 - Thyroid
 - Cervical esophagus

Level V: Spinal Accessory/Posterior Triangle

- These lymph nodes are posterior to the sternocleidomastoid muscle posterior margin and anterior to the anterior margin of the trapezius. They are arranged from cranial to caudal with the superior margin being the skull base and the inferior margin being the superior cortical surface of the clavicle. They can further be divided into VA above the cricoid and VB below the cricoid.
- Level V lymph nodes receive lymphatic drainage from:
 - Nasopharynx
 - Posterior neck
 - Posterior scalp

Level VI: Visceral

- The visceral lymph nodes are bounded by the hyoid bone superiorly and the medial aspects of the internal carotid arteries bilaterally.
- Level VI lymph nodes receive lymphatic drainage from:
 - Cervical esophagus
 - Thyroid
 - Larynx

6.3.2 Retropharyngeal Lymph Nodes

- Retropharyngeal lymph nodes are located anterior to the alar fascia at the level of the C1 vertebra and consist of medial and lateral lymph nodes.
- A short-axis diameter cutoff of 5–6 mm has been recommended as the size criterion for metastatic lateral retropharyngeal lymph nodes in adults or any node with central necrosis (Fig. 6.10).
- Retropharyngeal lymph nodes are larger in children than in adults. In particular, the mean size of lateral retropharyngeal lymph nodes is 7 mm in young children (Fig. 6.11), but these lymph nodes significantly shrink after 5 years of age.

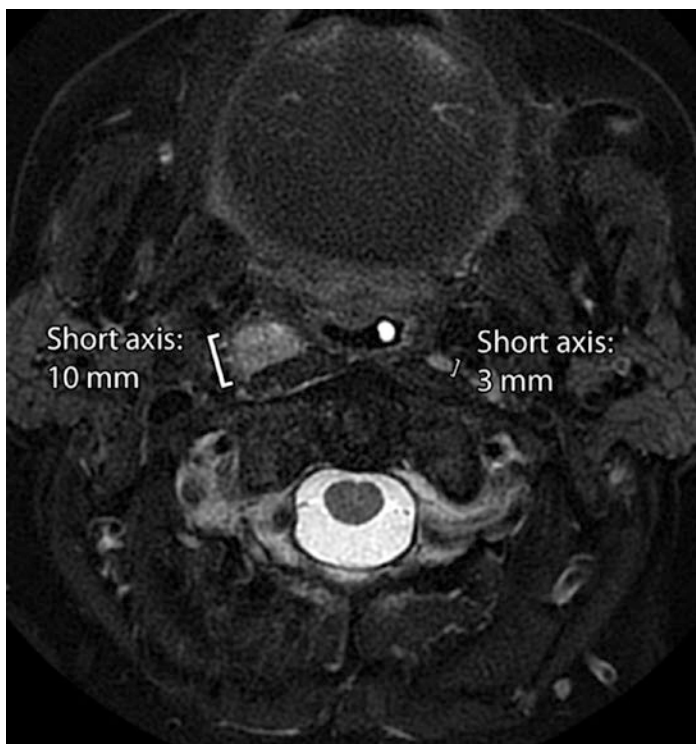


Fig. 6.10 Retropharyngeal lymphadenopathy. Axial fat-suppressed T2-weighted magnetic resonance imaging (MRI) shows a metastatic right lateral retropharyngeal lymph node that measures 10 mm in short axis and a normal left lateral retropharyngeal lymph node

- The medial retropharyngeal lymph nodes regress by adulthood.
- Retropharyngeal lymph nodes receive drainage from:
 - Nasal cavity
 - Paranasal sinuses
 - Upper pharynx
 - Oral cavity
 - Middle ear

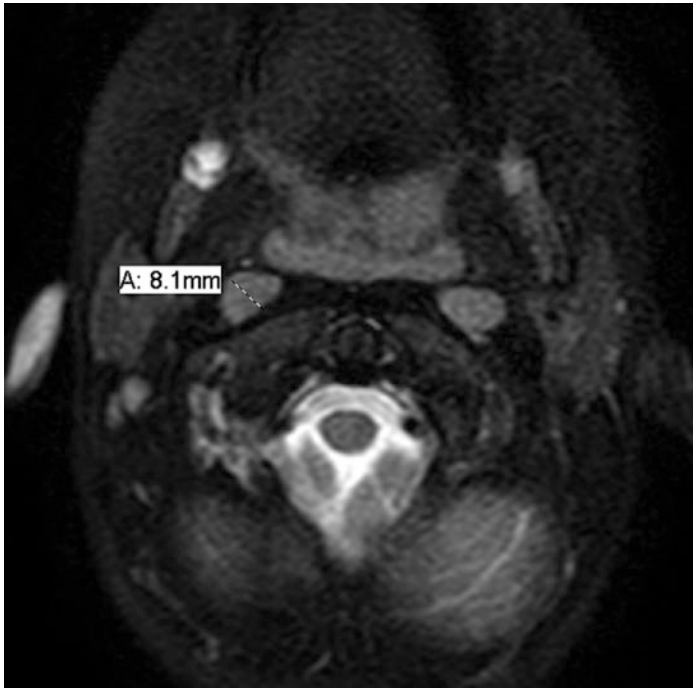


Fig. 6.11 Normal pediatric retropharyngeal lymph node. Axial fat-suppressed T2-weighted magnetic resonance imaging (MRI) shows lateral retropharyngeal lymph nodes that measure up to 8 mm in short axis

6.3.3 Parotid Lymph Nodes

- Parotid lymph nodes are comprised of superficial, extrafascial, subfascial extraglandular, and deep intraglandular nodes.
- The superficial extrafascial parotid lymph nodes are superficial to the superficial layer of the deep cervical fascia.
- The subfascial extraglandular group lymph nodes are deep to the fascia, but not in the parotid glandular tissue.
- The deep intraglandular lymph nodes are located within the parotid gland tissues, usually lateral to the retromandibular vein.



Fig. 6.12 Parotid lymphadenopathy. Axial computed tomography (CT) image shows a left face cutaneous squamous cell carcinoma with enlarged left parotid lymph nodes

- The average volume of normal parotid lymph nodes is 0.1 mL.
- A cutoff of 5 mm for the short axis of parotid lymph nodes has been proposed (Fig. 6.12).
- The parotid lymph nodes receive lymphatic drainage from:
 - Face and anterior scalp
 - Eyelids
 - Auricle and external auditory
 - Tympanic membrane and part of the Eustachian tube
 - Superficial preauricular lymph nodes
 - Posterior part of cheek
 - Parotid gland
 - Lacrimal glands

6.3.4 Occipital Lymph Nodes

- The occipital lymph nodes comprise the suprafascial, subfascial, and deep occipital node groups.
- The suprafascial or superficial group is intimately applied to the superficial layer of the deep cervical fascia or to the epicranial aponeurosis, along the occipital artery and great occipital nerve.
- The subfascial group lies near the superior nuchal line of the occipital bone, beneath the superficial layer of the deep cervical fascia.
- The deep occipital group lies beneath the superior insertion of splenius capitis, above the obliquus capitis superior, and medial to the longissimus capitis.
- Normal occipital nodes typically measure up to about 3–6 mm.
- Occipital lymphadenopathy can have an elongated morphology against the occipital bone (Fig. 6.13).



Fig. 6.13 Occipital lymphadenopathy. Axial computed tomography (CT) image shows enlarged lymph nodes in a patient with lymphoma

- Occipital nodes receive lymphatic drainage from:
 - Posterior part of the scalp
 - Posterior part of the upper neck

Further Reading

- Ahuja AT, Ying M. Sonographic evaluation of cervical lymph nodes. *Am J Roentgenol.* 2005;184:1691–9.
- Braams JW, Pruijm J, Freling NJM, Nikkels PGJ, Boering G, et al. Detection of lymph node metastases of squamous-cell cancer of the head and neck with FDG-PET and MRI. *J Nucl Med.* 1995;36(2):211–6.
- Chong V. Cervical lymphadenopathy: what radiologists need to know. *Cancer Imaging.* 2004;4(2):116–20.
- Chung MS, Choi YJ, Kim SO, Lee YS, Hong JY, Lee JH, Baek JH. A scoring system for prediction of cervical lymph node metastasis in patients with head and neck squamous cell carcinoma. *AJNR Am J Neuroradiol.* 2019;40(6):1049–54.
- Costa NS, Salisbury SR, Donnelly LF. Retropharyngeal lymph nodes in children: a common imaging finding and potential source of misinterpretation. *AJR Am J Roentgenol.* 2011;196(4):W433–7.
- Costa E, Silva Souza LMB, Leung KJ, O'Neill A, Jayender J, Lee TC. Jugulodigastric lymph node size by age on CT in an adult cancer-free population. *Clin Imaging.* 2018;47:30–3.
- Curtin HD, Ishwaran H, Mancuso AA, Dalley RW, Caudry DJ, McNeil BJ. Comparison of CT and MR imaging in staging of neck metastases. *Radiology.* 1998;207:123–30.
- Dooms GC, Hricak H, Crooks LE, Higgins CB. Magnetic resonance imaging of the lymph nodes: comparison with CT. *Radiology.* 1984;153(3):719–28.
- Eisenmenger LB, Wiggins RH III. Imaging of head and neck lymph nodes. *Radiol Clin North Am.* 2015;53(1):115–32.
- Lengelé B, Hamoir M, Scalliet P, Grégoire V. Anatomical bases for the radiological delineation of lymph node areas. Major collecting trunks, head and neck. *Radiother Oncol.* 2007;85(1):146–55.
- Leticia MB, Souza CS, Leung KJ, O'Neill A, Jagadeesan J, Lee TC. Jugulodigastric lymph node size by age on CT in an adult cancer-free population. *Clin Imaging.* 2018;47:30–3.
- Lim RS, Ramdave S, Beech P, Billah B, Karim MN, Smith JA, Safdar A, Sigston E. Utility of SUVmax on 18 F-FDG PET in detecting cervical nodal metastases. *Cancer Imaging.* 2016;16(1):39.
- Maeda T, Yamamoto Y, Furukawa H, Oyama A, Funayama E, Murao N, Hayashi T. Dominant lymph drainage patterns in the occipital and parietal

- regions: evaluation of lymph nodes in patients with skin cancer of the head. *Int J Clin Oncol*. 2017;22(4):774–9.
- Nishio N, Fujimoto Y, Hiramatsu M, Maruo T, Tsuzuki H, Mukoyama N, Yokoi S, Wada A, Kaneko Furukawa M, Furukawa M, Sone M. Diagnosis of cervical lymph node metastases in head and neck cancer with ultrasonic measurement of lymph node volume. *Auris Nasus Larynx*. 46(6):889–95. pii: S0385-8146(18)30489-9.
- Norling R, Buron BMD, Therkildsen MH, Henriksen BM, von Buchwald C, Nielsen MB. Staging of cervical lymph nodes in oral squamous cell carcinoma: adding ultrasound in clinically lymph node negative patients may improve diagnostic work-up. *PLoS One*. 2014;9:e90360.
- Sathyanarayan V, Bharani S. Enlarged lymph nodes in head and neck cancer: analysis with triplex ultrasonography. *Ann Maxillofac Surg*. 2013;3(1):35–9.
- Seymour L, Bogaerts J, Perrone A, Ford R, Schwartz LH, et al. iRECIST: guidelines for response criteria for use in trials testing immunotherapeutics. *Lancet Oncol*. 2017;18:e143–52.
- Shetty SK, Harisinghani MD. Magnetic resonance techniques in lymph node imaging. *Appl Radiol*. 2004; accessed online. <https://appliedradiology.com/articles/magnetic-resonance-techniques-in-lymph-node-imaging>.
- Som PM. Detection of metastasis in cervical lymph nodes: CT and MR criteria and differential diagnosis. *AJR Am J Roentgenol*. 1992;158(5):961–9.
- Spector ME, Gallagher KK, Light E, Ibrahim M, Chanowski EJ, et al. Matted nodes: poor prognostic marker in oropharyngeal squamous cell carcinoma independent of HPV and EGFR status. *Head Neck*. 2012;34(12):1727–33.
- Sun J, Li B, Li CJ, Li Y, Su F, Gao QH, et al. Computed tomography versus magnetic resonance imaging for diagnosing cervical lymph node metastasis of head and neck cancer: a systematic review and meta-analysis. *Onco Targets Ther*. 2015;8:1291–313.
- Van den Brekel MWM, Stel HV, Castelijns JA, Nauta JJP, van der Waal I. Cervical lymph node metastasis: assessment of radiologic criteria. *Radiology*. 1990;177:379–84.
- Van den Brekel MWM, Castelijns JA, Snow GB. The size of lymph nodes in the neck on sonograms as a radiologic criterion for metastasis: how reliable is it? *AJNR Am J Neuroradiol*. 1998;19:695–700.
- Vandecaveye V, de Keyzer V, Dirix P, Verbeken E, Nuyts S, Hermans R. Head and neck squamous cell carcinoma: value of diffusion-weighted MR imaging for nodal staging. *Radiology*. 2009;251:134–46.
- Veenstra HJ, Klop WM, Lohuis PJ, Nieweg OE, van Velthuysen ML, Balm AJ. Cadaver study on the location of suboccipital lymph nodes: guidance for suboccipital node dissection. *Head Neck*. 2014;36(5):682–6.

- Ying M, Ahuja A, Brook F, Brown B, Metreweli C. Sonographic appearance and distribution of normal cervical lymph nodes in a Chinese population. *J Ultrasound Med.* 1996;15(6):431–6.
- Ying M, Ahuja A, Brook F. Sonographic appearances of cervical lymph nodes: variations by age and sex. *J Clin Ultrasound.* 2002;30(1):1–11.
- Zhang GY, Liu LZ, Wei WH, Deng YM, Li YZ, Liu XW. Radiologic criteria of retropharyngeal lymph node metastasis in nasopharyngeal carcinoma treated with radiation therapy. *Radiology.* 2010;255(2):605–12.
- Zhang MH, Ginat DT. Normative measurements of parotid lymph nodes on CT imaging [published online ahead of print, 2020 May 14]. *Surg Radiol Anat.* 2020;10.1007/s00276-020-02494-8. <https://doi.org/10.1007/s00276-020-02494-8>.